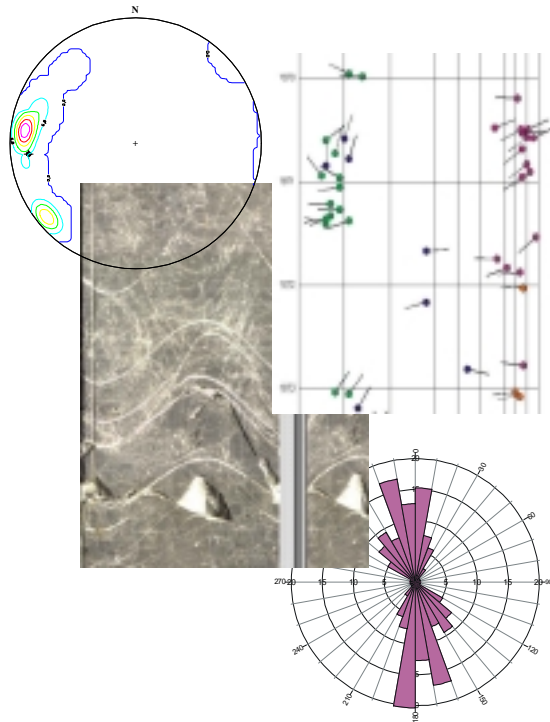




CORE FRACTURE DESCRIPTION DEMO WELL ANALYSIS



Prepared by

CORIAS

January 2000

1. INTRODUCTION.

2. PRINCIPLE OF ANALYSIS.

2.1. Individualisation of scribe-lines.

2.2. Data collection.

2.2.1. The sedimentary features.

2.2.2. The tectonic features.

2.2.3. The induced fractures.

2.3. Reorientation operations.

3. RESULTS AND INTERPRETATION.

3.1. Presentation of the results.

3.2. 3.2. Analysis of data.

3.2.1. Sedimentary spatial organisation

3.2.2. Fracturing spatial organisation.

3.2.3. Induced fractures

4. CONCLUSION

5. FRACTURE POROSITY AND PERMEABILITY.

5.1. Fractures frequency

5.2. Frequency computing

5.3. Porosity computing

5.4. Permeability computing

5.5. Finding the “best” direction for a production well

1. INTRODUCTION.

An extensive structural core analysis was carried out on 'DEMO1' well on 'XXX' field. The aim of the study was the generation of graphical documents used to study the structural characteristics of the cores. The data acquisition took place on the drilling site.

The very good quality of the cores, carried in the fibre glass tubes, allowed a detailed and complete structural core analysis for the complete cored zone. Special precautions, during cutting of cores in metrical pieces, allow a good fitting of core fragments for the whole well.

The cores were oriented using the **Corpro** coring technique with electronic survey system 'EMS', giving the real orientation of the cores.

2. PRINCIPLE OF ANALYSIS.

2.1. *Individualisation of scribe-lines.*

The acquisition of geological data is done with a fine accuracy, so one of our first attention was to check the physical joining of all the different pieces constituting the studied cores and the integrity of the scribe-lines. Thus, a long and important work consist of the reconstitution of the cores, in fragments with a maximum connected length.

A scribe-line was drawn on each fragment. In order to perform this operation, it became necessary to draw only 3 scribe-lines for the whole studied zone, separated by non connected breaks.

2.2. *Data collection.*

The collection of data has been done with a 3D structural analyser. This system allows a direct on core acquisition and computer recording of the co-ordinates of all planes and lines present on cores. This procedure is based on a 3D digitisation operation. A coupled software package allows entry of geological descriptions of planes and instantaneous drawing of all types of diagrams.

The collected data are first oriented by reference to the scribe-lines and, after treatment, will be restored in the real geographic position. For the 54 meters of studied cores, 574 data have been collected.

2.2.1. The sedimentary features.

The sedimentary planes have been divided into 4 types:

- **Bedding Planes** : They show the stratification materialised by colour or grain size variations.
- **Sedimentary Stylolites** : thin joints with a thickness of 1/10 of millimetre, undulated by stylolitization. The vertical stylolitic teeth have an amplitude from a few millimetres to 2 or 3 centimetres. They constitute the most common sedimentary planes in the study.
- **Anhydrite Limits**: planes in geometrical disconformity with the bedding planes and other planes. In the present case these planes have been used only to give the position of anhydrite zones.
- **Stratification Joints**: joint with a thickness varying from 1 to 5 millimetres. These planes generally consist of clay.

2.2.2. The tectonic features.

2 types of tectonic structures are recorded:

- **open fractures**: thin open diaclases, generally sub vertical and visible along several centimetres. Their opening is about 0.1 to 0.8mm.
- **gashes**: thin fissures with calcite filling. These structures are completely consolidated. Only 2 of these structures have been recorded.

2.2.3. The induced fractures.

These fractures are developed during or after coring. The development of induced fractures is under the control of pre-existing mechanical anisotropy (natural fractures and bedding planes). Their orientation is influenced by in-situ stress. These fractures are generally observed in the fine-grained and competent rocks. These planes present generally moderate dip values, around 60° and present a characteristic minor representation in the core volume.

2.3. Reorientation operations.

The original data obtained from the reference scribe-lines are computed and restored in their real spatial position by a reorientation process taking in account the orientation data.

The cores are grooved by three knives as they are going into the core barrel. These knives are separated by three different angles (100°, 120° and 140°), and one of them is the reference groove. This groove will be used as reference line to make the measurement of the structures on cores (the reference line drawn on the cores is oriented in reference with this groove).

A multishot instrument is set within a non magnetic collar above the core barrel and aligned with the reference groove. Survey data are shot throughout the course of drilling providing orientation of the entire core. The tectonic and sedimentary data picked up in reference to the orientation groove are replaced in geographical position by using the core orientation data that are delivered in a tabular format with the depth.

To circumvent this problem, a simple graphical display of the orientation of the reference groove with the depth in standard trip log format has been developed.

3. RESULTS AND INTERPRETATION.

3.1. *Presentation of the results.*

Format used for presentation are:

- **logs - dipmeter log scale 1/40**

Remark: on the log, each type of sedimentary and tectonic structure is differentiated by the use of specific colours and shape code. The position of the oil zones is also provided on this log. These zones have been localised by use of a ultra-violet lamp directly on the site.

- **stereonet plots;** used for the tectonic planes and induced fractures and sedimentary planes
- **rose diagrams,**
- **strike rose diagrams;** used for the tectonic planes and the induced fractures,
- **azimuth rose diagrams;** used for the sedimentary azimuths
- **frequency dip angle histograms;** used for the organisation of tectonic and sedimentary dips

Remark: For all the diagrams, the dip directions values of sedimentary planes with a dip value less than 2 degrees were not taken in account. These planes can be considered as horizontal. This is justified because the precision of planeity on real geological planes is low.

3.2. *Analysis of data.*

The main dip direction and strike direction are defined. The dip values are studied.

3.2.1. **Sedimentary spatial organisation**

The general sedimentary organisation for each core is obtained by analysis of bedding planes and stylolites orientations. The stylolites are sometimes quite in discordance with bedding, so they give complementary information.

The bedding planes rose diagram shows that the azimuths are towards NW but a **N50 (N-E) trend** exist. Two secondary opposite trends in N300 and N120 are also noticed. The azimuths of sedimentary stylolites show also a good trend from N350 to N60. So the main trend for these planes is near the bedding trend towards N-E. The azimuths of stratification joints show a trend towards North. (fig1)

The histogram of bedding planes shows that the dips have generally low to medium values with an **average of 8°**. The sedimentary stylolites and stratification joints present also low average values, a little bit higher, around 10° (fig2).

3.2.2. **Fracturing spatial organisation.**

There are 118 data which have been recorded. These planes are not really important fractures. Their length on core do not exceed 20cm for the most important.

The open fractures rose diagram shows a remarkable **trend North-South** (between N165 and N190), and a **second direction centered in N135**. (fig3). The stereonet plot (fig4) shows that the majority of fractures have a dip towards West.

The dip histogram shows that the dips could have high values near 80°, but some fractures present medium values between 60° and 70°.

3.2.3. Induced fractures.

Rose diagram and stereonet plot show that the induced fractures present a clear **NNW-SSE (N160) trend** and some NNE-SSW values. Dips range between 50° and 80° with an average of 75°.

Generally, these induced fractures appear in a direction parallel to the maximum in situ stress and perpendicular to minimum stress.

The principal induced fractures trend is closely parallel to the open fracture trend. This could mean that some open fractures in N160 to N170 direction are parallel to the maximum in situ stress and that they should be open in situ. This confer to open fractures in this direction an important role of drain. On the contrary, fractures perpendicular to the main trend of induced fractures should have a role of permeability barriers.

4. CONCLUSION

The outstanding points are:

- For sedimentary planes: a good N50 main trend and two secondary trends N300 and N120, dip values are around 8°.
- For the tectonic planes, one major trend for open fractures in N0 and a second in N135. Dips present values between 65 to 85°.

Induced fractures let us define a **NNW-SSE trend**. This could be the direction of the maximum horizontal in situ stress. It could confer to the open fractures in this direction an important role of drain.

5. FRACTURE POROSITY AND PERMEABILITY

5.1. *Fractures frequencies*

Why computing fracture frequencies?

Usually, geological core studies take in account the **number of fractures** encountered **each meter** along the bore-hole in order to compute what can be called the **fracture density**, [frac/m]. The interpretation of such information often leads to erroneous result when one tries to figure out the real spatial (3D) pattern of a faulted medium.

Let us considered the faulted rock medium of **figure 5** where two families of faults occur: F1 sub-horizontal and F2 sub-vertical.

The rose diagram drawn on the upper right corner seems to indicate that the F1 direction is the main one.

While watching this figure it is obvious that such a suggestion is far from easy to catch as unreliable. In order to avoid this problem, we prefer to compute the so called fracture frequency (inverse of spacing) which is the number of fractures counted each meter in a direction perpendicular to a specific fracture family.

In this way the shape of the rose diagram (low right corner) will fit the real fracture pattern of the rock mass, where the family F2 is obviously the main one.

Another major application of the **fracture frequency** is for the computation of **fractures porosity** and **permeability tensor**. Therefor we propose to define the major trends of the fracture families and to represent their frequencies in logs.

5.2 *Frequency computing*

Methodology:

To find the different families of fractures we use the Azimuth rose diagram combined to the stereographic projection depending on the data. From the strike rose diagram, there are 2 major families of fracture: N0 and N135.

From the azimuth rose diagram and the stereonet, 4 families of fractures have been selected as listed bellow (**Table I**) to make the calculation of frequencies.

TABLE I :Listing of the fractures families.

Family	Azi	Dip	Azi Min	Azi Max	Famdir
F1 =	49	88	25	65	N0
F2 =	230	74	205	245	N0
F3 =	91	75	65	115	N135
F4 =	268	75	245	295	N135

Azi= Azimuth; Dip= Dip;

For each of these families, the spatial frequency has been computed and represented by a log. For the convenience, the families presenting the same strike but an opposite dip direction, have been combined. That is why we give only 2 logs which summarise the results. All data are plotted on figure 6.

GEOLOGICAL IMPLICATION

- There is a small heterogeneity in the spatial distribution of fracture frequencies, the highest fractured zone are located between 1865 to 1875m and 1879 to 1888.
- The main fracture directions is **N0**, the frequencies are 5 to 26 between 1879 and 1883. There is also a maximum of frequency in the direction N135, at 1870.50, this is due to a high density of small fractures.
- So major fractured zone exists between 1870m and 1883m.

5.3. Porosity computing:

The porosity is computed, according to the following statements:

- In general the **core characteristics** are supposed to be **reliable** for at least one **cubic meter of rock centred on the core** (the core crosses the cube of rock from its upper to its lower face). Therefore the porosity values refer to one cubic meter of rock and they are computed every meter along the bore-hole.
- The **surface** of the fractures is at least **one square meter**. Such a statement shall be regarded as an approximation because in reality fractures are frequently stopped by other fractures and the real shape of the surface of the fracture is a complex polygon.

On the other hand, the existence of a relation between the length and the aperture of a fracture is a widely admitted fact. Usually there is concomitant increase of both parameters, but in reality this relation is much more complex, changing from case to case.

Thus the length error will preferably affect the “small” apertures, with length under a meter. Inside a fractured block, the influence of the “small” open fractures is minor when compared with the influence of “large” open fractures and consequently the error in the calculated porosity values will be reduced.

- The calculation is done by **cumulating** of the porosity of all **individual fracture families**. Furthermore the **porosity of every fracture family** is computed from the above cumulating.
- Concerning the opening of fractures: the **fractures aperture** values are recorded **directly on the site** by the operator of the AS3D analyser. The **thickness of each fracture** is supposed to **be constant** and should be already “averaged” by the operator (in case of partial opening, like “**bridge fractures**”, only the **effective opening** is used).

Regarding the **opening of fractures belonging to one family** there are two approaches:

When the bore-hole length is limited, the opening of fractures is considered as constant for the whole bore-hole length. When the length of the bore-hole is “important”, the opening is considered as a constant only in for every successive cubic meter of rock along the bore-hole or for a specific depth portion. Thus for every fracture family the average opening (Avg) and the standard deviation (Std) of the opening will be computed.

TABLE II : Listing of the mean openings.

Family	Avg Azi [°]	Avg Dip [°]	Avg Open [mm]	Std Open [mm]
F1 =	49	88	0.08	0.00
F2 =	230	74	0.07	0.01
F3 =	91	75	0.07	0.01
F4 =	268	75	0.06	0.02

Avg= Geometric mean; Std= Standard deviation.

Remark .According to the stress in situ, to compute, we apply a 0.3 factor to the opening which was measured by the operator.

Conclusion

The fractured zones bear a low to medium porosity, in the most important fractured zone, between 1870m and 1883m, the porosity have values around **0.05 and 0.16%**. The highest fracture porosity value is **0.28%** at 1870.5 depth. (fig7).

5.4. Permeability computing:

The permeability will be calculated making some additional statements:

The **fractures length** is supposed to be “**infinite**” or in reality when there are more than one fracture systems, the fractures belonging to one set are intercepted by the others, resulting into a considerable length.

Concerning that hypothesis one should be surprised, but some recent research works show that when at least two systems of fractures exist and if their frequencies reach 4F/m the influence of their length (>1m) could easily be neglected. Especially when compared with the uncertainty on the opening on the permeability.

The flow is generally regarded as **non turbulent** and the **POISEUILLE** law is **applied**. Only in the case of gas there is a non laminar flow transition zone and the formula of **LOMIZE** is applied (**KIRALY**² 1971).

The relative coefficient of rugosity has a medium value for oil and a high value for gas.

- The codes used for the computation of the fracture frequency have been derived from the **permeability tensor theory** (**KIRALY**¹ 1971). This theory gives an accurate approximation of the reality and is scientifically recognised as reliable regarding the base hypothesis (not too restrictive). The results are given in the figure 7.

By the use of all these hypothesis, we draw a permeability log, where 3 ranges of data represent the module of the maximum (K1), mean (K2) and minimum (K3) permeability vector.

The values of permeability are high, only the interceptibility of the values along the well is significant. An other important point is that the opening measured on cores, probably quite often refer to voids and we should try to minimise them in a certain way before extending them to the reference 1 square fracture surface.

Again the permeability shows many maximum, with a highest value of 1155Md at depth 1870.50m. But as for first approximation we could conclude that the most interesting zone is the fractured zone between 1870 and 1895m which shows a specific comportment and is reliable to the frequency and porosity increasing.

To the best use of these result it is important to search the relation between fractures and oil zones (see log in annex 1). In regard to this point it seems that the best zones should be between 1870 and 1880m and also between 1898 and 1905.

An other important point is the position of oil zones in relation to the sedimentary stylolites. At this step of the study it is not possible to give a final conclusion. It is necessary to compare the position of fractures and stylolites in the well.

¹)**KIRALY L.** 1971:- Groundwater flow in Heterogeneous, Anisotropic, faulted media: Journal of Hydrology 12 p. 255-261.

5.5. Finding the “best” direction for a production well.

In an anisotropic pervious rock medium, such as a fractured reservoir, the **best orientation** of a well for the most efficient **drainage** of an oil field, could be **deduced from the orientation** of the **permeability ellipsoid**.

Thus, the **orientation** of a **production well** should be **perpendicular** to the **K1,K2** plane and **parallel to the K3** vector. **Statistically the best spatial** distribution of the K3 vector is found drawing a **K3 density stereonet** and determining the mean lineation vector (**Figure 8**).

The mean K3 vector's orientation, which indicates in a theoretical (statistical) way the “best spatial position” of a production well, deduced from the core fractures analysis, is plotted on this figure.

Thus the “**ideal**” **position** of the well will be almost close to this mean vector, may be somewhere close to the azimuth N84, with plunge of 14° towards NE.

But considering the important effect of the stylolite in the distribution of the oil zones this conclusion has to be reconsidered. So it seems that the best way to drill the most efficient well should be in the N80 direction with horizontal dip. Considering the azimuth trend of stylolites the azimuth of drilling should be **towards N260**.

LIST OF FIGURES

FIGURE 1: Azimuth rose diagram of sedimentary planes

FIGURE 2: Dip angle histogram of bedding planes

FIGURE 3: Strike rose diagram of tectonic planes

FIGURE 4: Stereonet plot of tectonic planes

FIGURE 5: Comparison between frequency and density of fractures of an experimental drill-hole

FIGURE 6: Frequency log, N0 and N135 direction

FIGURE 7: Porosity and permeability log, mean aperture

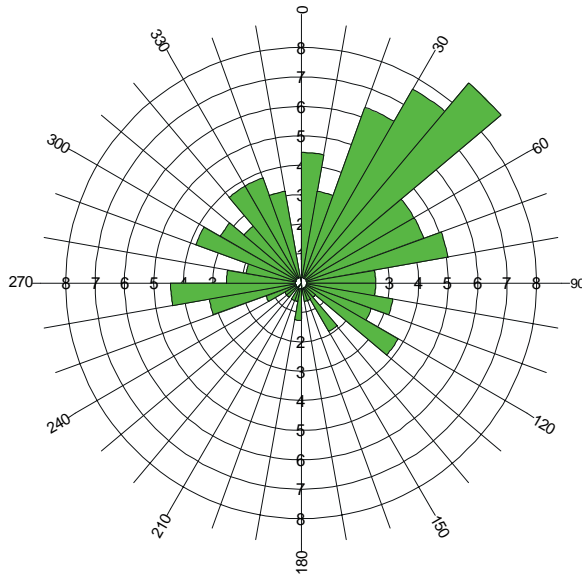
FIGURE 8: Density stereonet, K3 permeability tensor

LIST OF ENCLOSURES

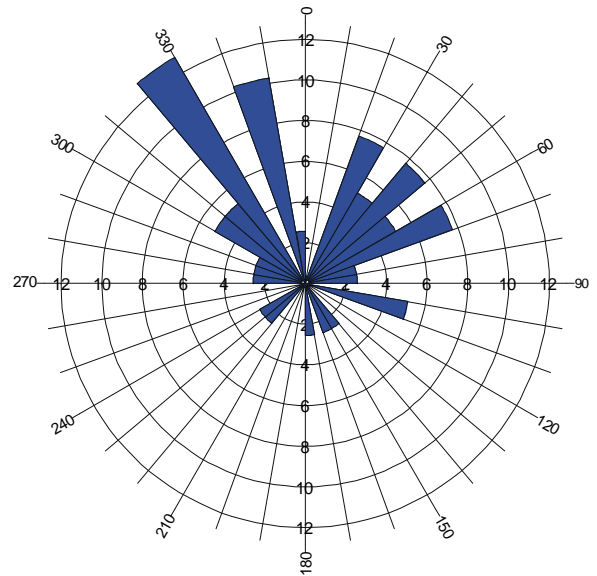
ENCLOSURE 1: Dipmeter log 1/40 scale

FIGURE 1
DEMO 1

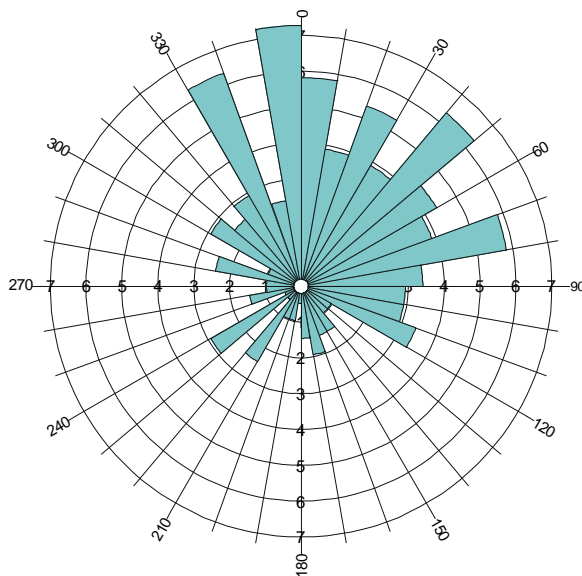
Azimuth rose diagrams



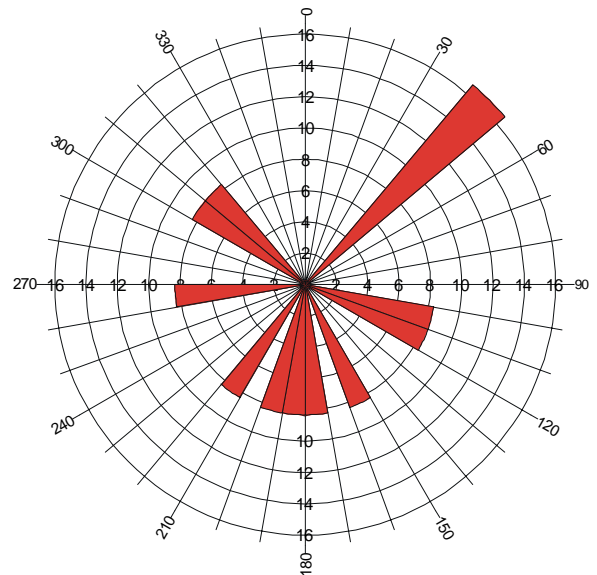
152 data
BEDDING PLANES



196 data
SEDIMENTARY STYLOLITHES

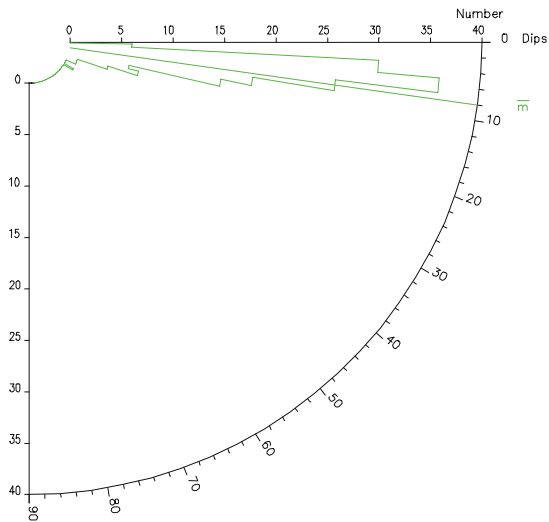


38 data
STRATIFICATION JOINTS

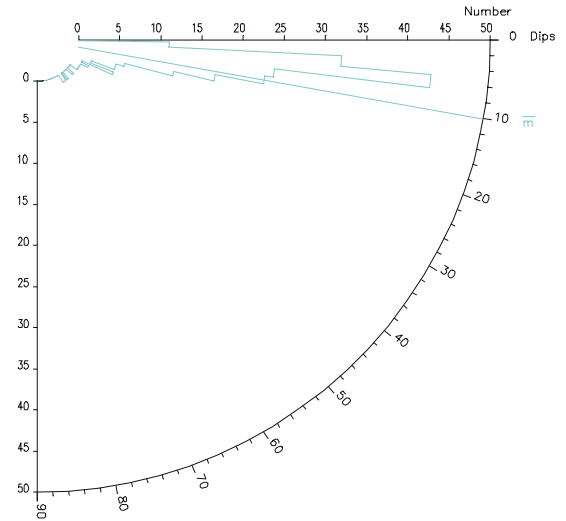


11 data
ANHYDRITE

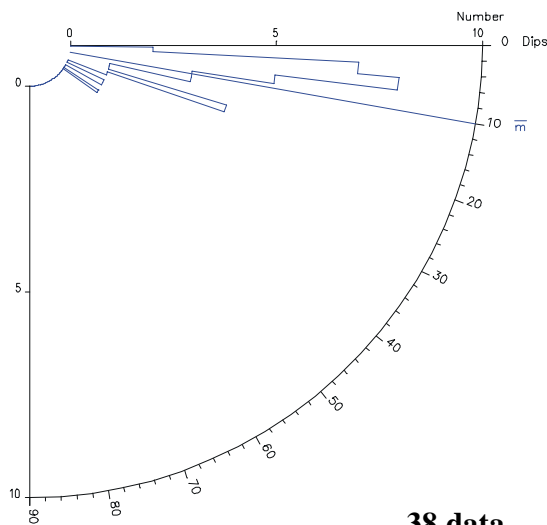
FIGURE 2
DEMO 1
Dip histograms



152 data
BEDDING PLANES



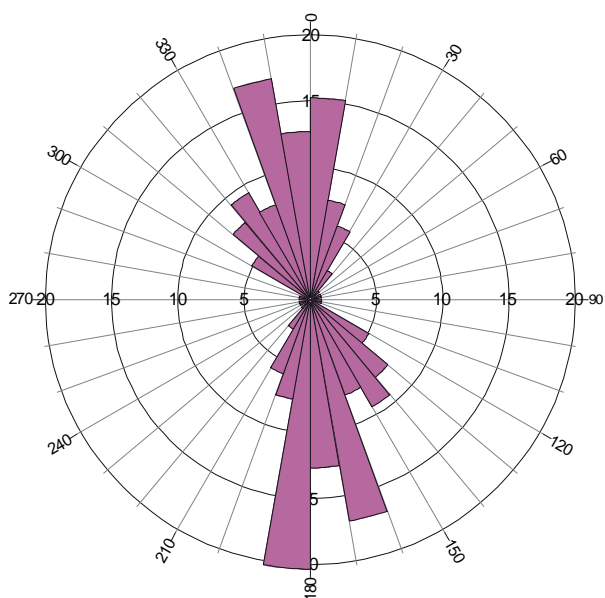
196 data
SEDIMENTARY STYLOLITHES



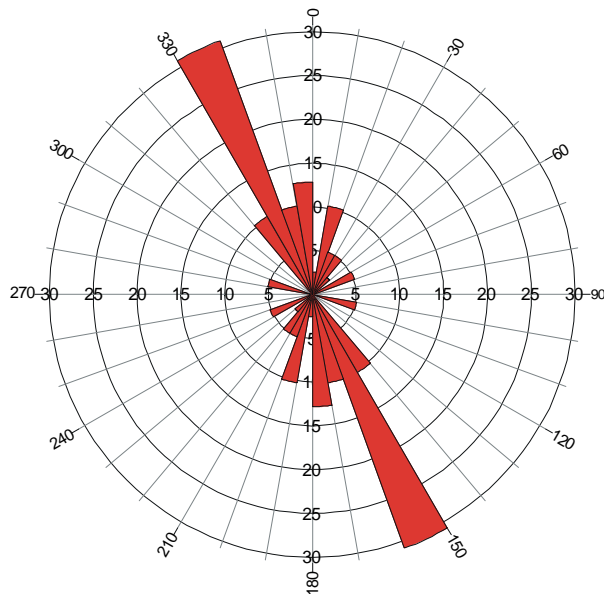
38 data
STRATIFICATION JOINTS

FIGURE 3
DEMO 1

Strike rose diagrams and dip histograms



118 data
OPEN FRACTURES



39 data
INDUCED FRACTURES

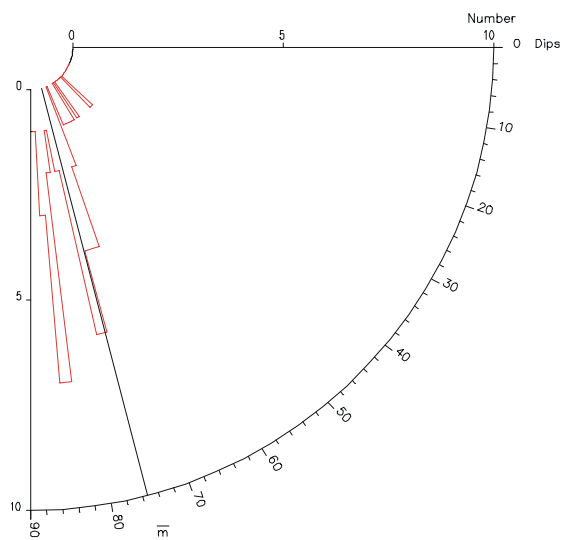
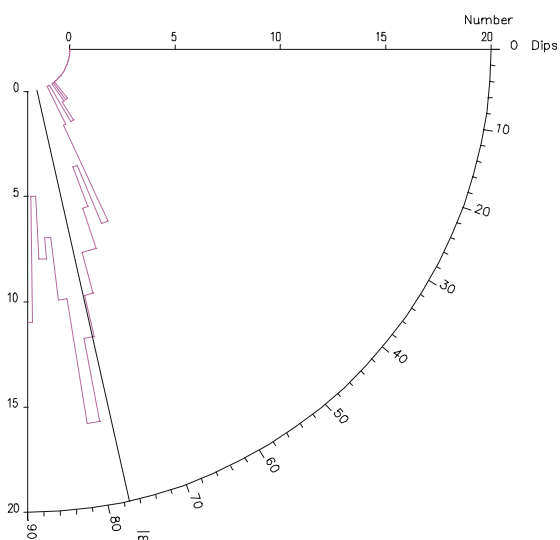
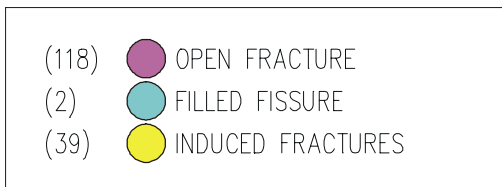
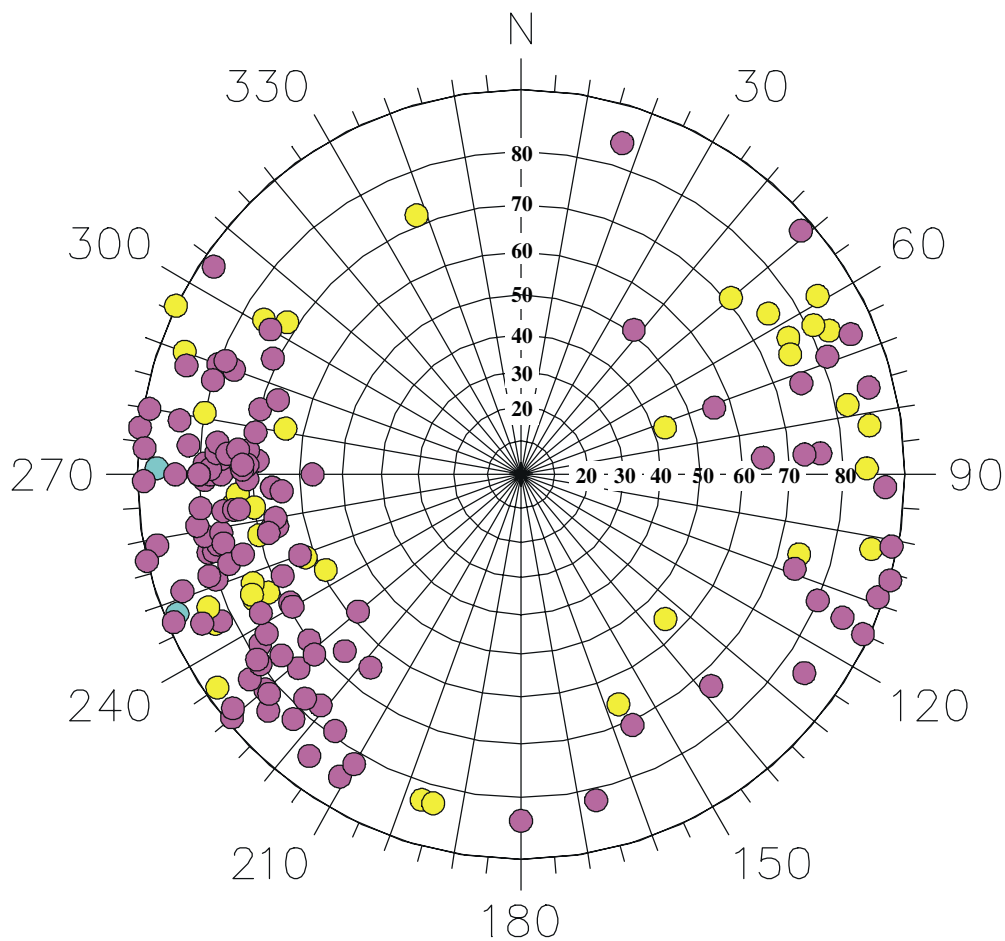


FIGURE 4

DEMO-1

Stereonet plot

Tectonic planes



CORES 1 to 3
From 1862m to 1917m
Corrected data
159 DATA

STEREOGRAPHIC PROJECTION - WULFF NET - UPPER HEMISPHERE

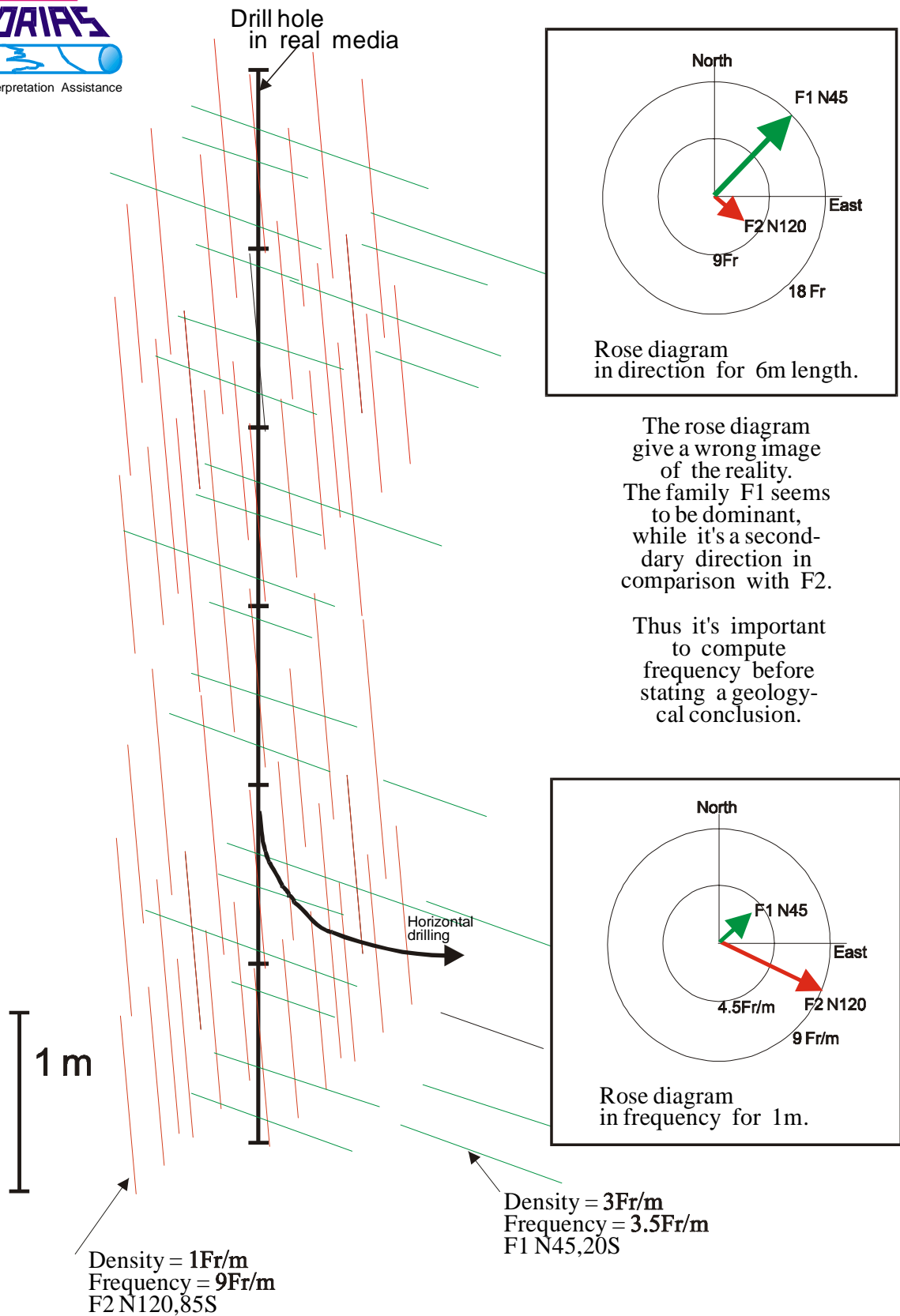


Figure 5

FIGURE 6
DEMO-1

Fracture Frequency and Density

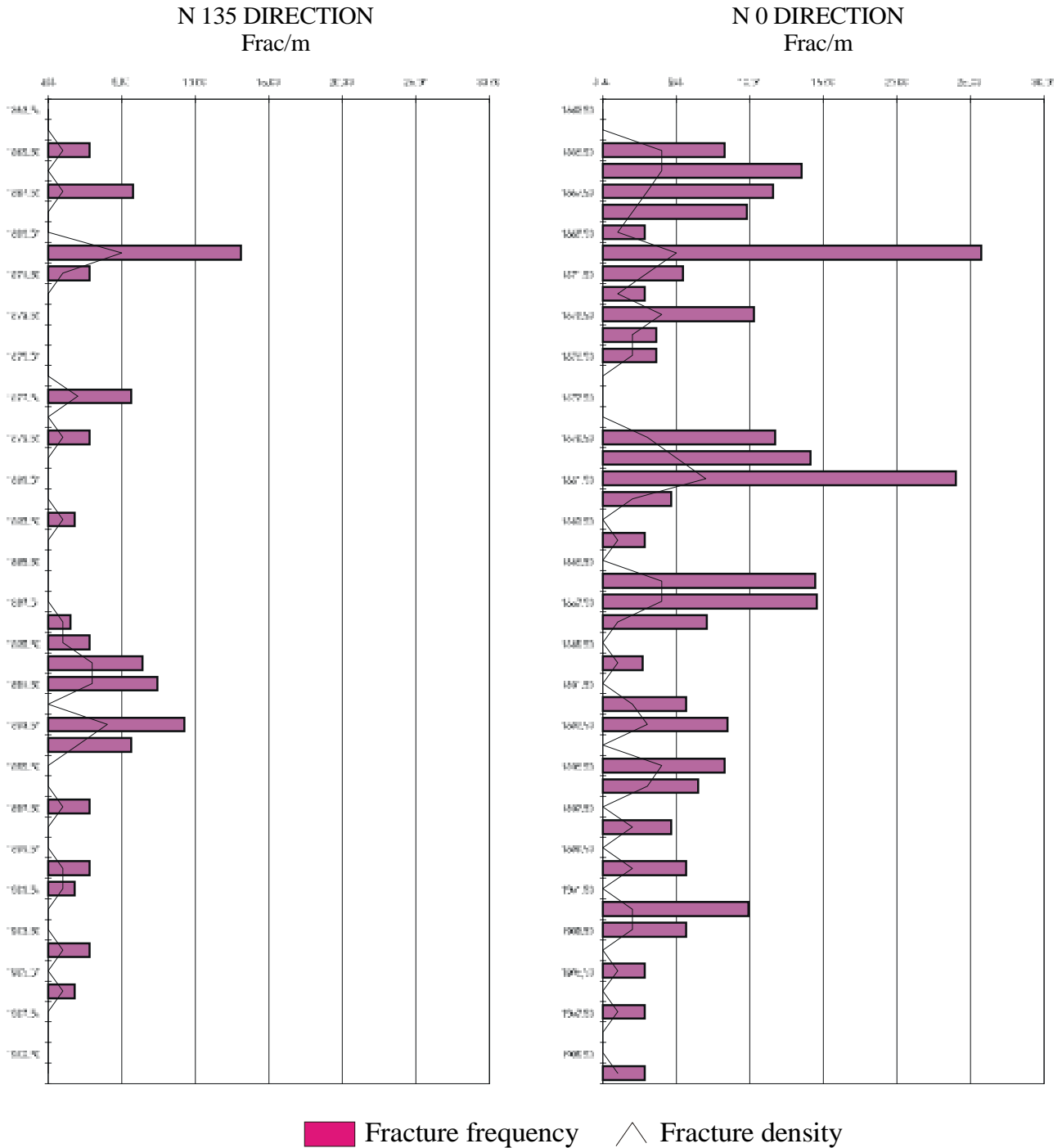




FIGURE 7
DEMO-1

Fractures porosity and permeability

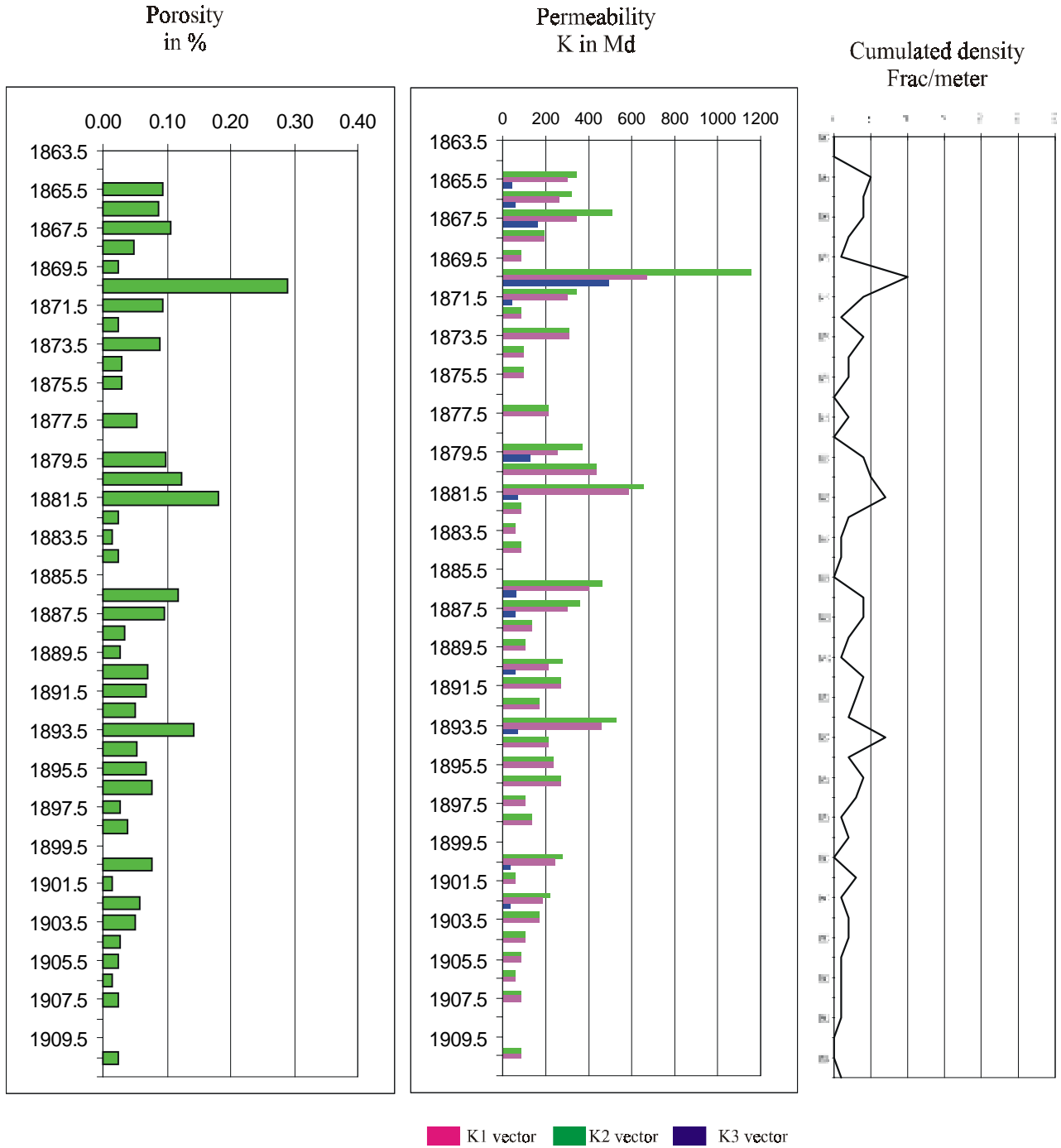
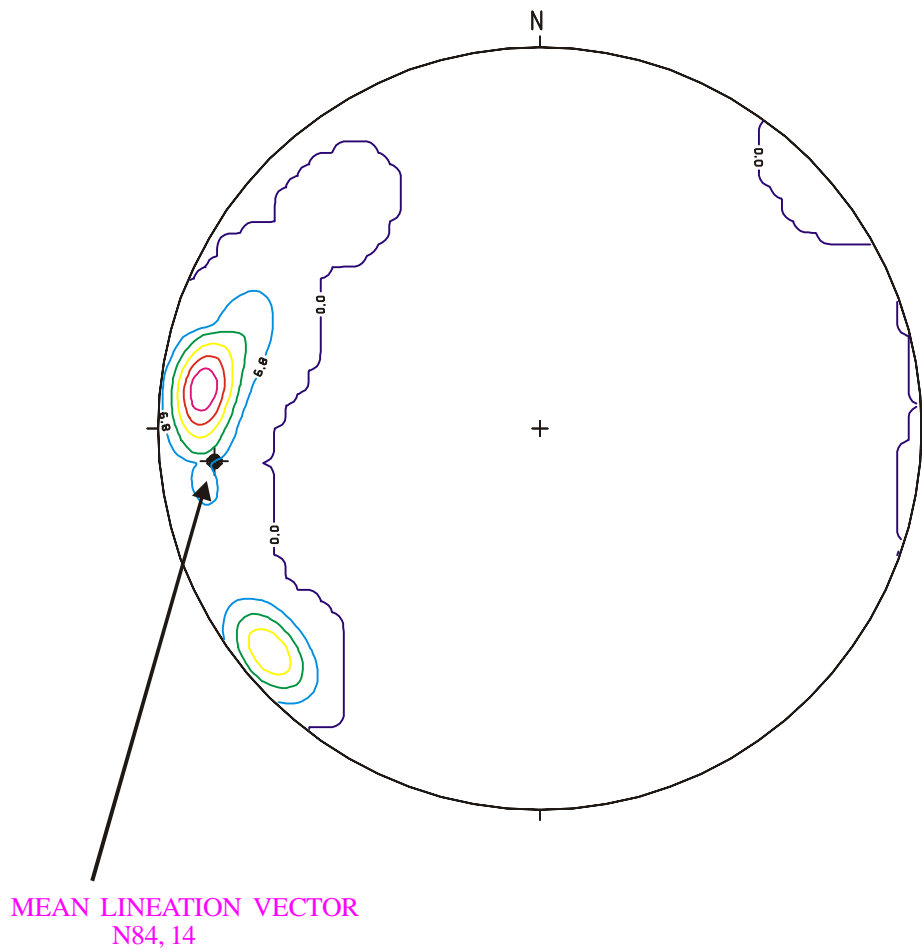


FIGURE 8
DEMO-1

Density stereonet
K3 permeability vector



schmidt net - upper hemispher